Available online at www.sciencedirect.com

ScienceDirect

Energy Procedia 38 (2013) 86 – 93

Energy Procedia

SiliconPV: March 25-27, 2013, Hamelin, Germany

Application of a new ray tracing framework to the analysis of extended regions in Si solar cell modules

Hendrik Holst[a,*], Matthias Winter[a,b], Malte R. Vogt[b], Karsten Bothe[b], Marc Köntges[b], Rolf Brendel[a,b], Pietro P. Altermatt[a]

[a] *Institute of solid-state physics, Dep. Solar Energy, Leibniz University Hannover, Appelstr. 2, 30167 Hannover, Germany*
[b] *Institute for Solar Energy Research Hamelin (ISFH), Am Ohrberg 1,31860 Emmerthal,Germany*

Abstract

While ray tracing of solar cells was established decades ago, ray tracing of entire modules has met obstacles, mainly because module optics are affected by geometric structures varying over a large scale of dimensions. In this paper, we introduce a ray tracing framework that is based on a modular structure made up of separate plugins. While existing plugins can be used for common effects such as light sources, absorption in materials, etc., specialized plug-ins can be written by users to handle problem-specific properties. We demonstrate the functionality of our approach by ray tracing a test module containing 9 crystalline Si solar cells. Good agreement between light-beam induced current (LBIC) measurements and ray tracing is achieved.

Keywords: ray tracing; module; LBIC

1. Introduction

While cell optics were heavily studied by ray tracing simulations [1-6] during the last decades, full ray tracing simulations of solar cell modules are more difficult to perform. To the best of our knowledge, this task has been performed with simplifications [7-8] or by analytical approaches such as in Ref. [9], for two main reasons: firstly, the optics of solar cell modules is determined by geometric structures on a wide scale of dimensions, ranging from pyramids on cells in the micrometer range to module geometry in the

* Corresponding author. Tel.: +49-5151-999-644; fax: +49-5151-999-400.
E-mail address: holst@isfh.de

doi:10.1016/j.egypro.2013.07.253

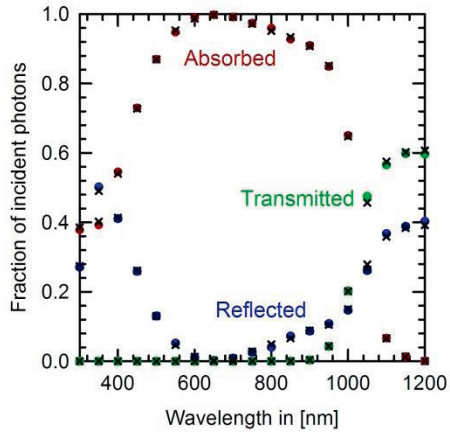

Fig. 1. Absorbance, reflectance and transmittance of a 170µm thick polished silicon wafer with a 79 nm thick SiN_x coating on its front side, ray traced with DAIDALOS(crosses) and SUNRAYS(circles) Very good agreement between SUNRAYS and DAIDALOS is achieved.

centimeter range. This leads to high complexity of the simulation. Secondly, although it would be possible to accelerate these simulations by exploiting specific properties, the code of available ray tracing software is rather hard to extend to serve this purpose.

We therefore developed a ray tracing framework called DAIDALOS, providing a modular structure, fully based on separate plugins. We demonstrate the functionality of our approach by simulating a test module and comparing the tracing results with light-beam induced current (LBIC) measurements.

2. The DAIDALOS –Framework

The DAIDALOS ray tracing framework was developed to be as highly configurable as possible. In the first instance, this means the whole framework is written in the Java programming language, in order to make it almost independent of the platform on which it runs.

Additionally, the framework is not programmed as monolithic application. Instead, it is based upon many smaller parts of programming code, so called plugins. While the framework provides a base of plugins for common effects, e.g. light sources, the user is always able to extend it by adding self-written plugins. Following this approach, any part of a ray tracing simulation, even the ray tracer itself, may be replaced by a user-written one for performance reasons or to integrate new effects. Up to now, the framework and its plugins were extensively tested by comparison with the well-known ray tracer SUNRAYS [3]. An example is shown in Fig. 1 for the case of a polished Si wafer, having a 79 nm thick SiN_x coating on its front side. Very good agreement between SUNRAYS and DAIDALOS is achieved.

2.1. Simulation process

In order to simplify the preparation of new simulations as well as the development of new plugins, the DAIDALOS framework has been developed to consist of two separated branches. First of all, the preparation of new simulations is supported following a three step process as indicated in Fig.2. (i) The simulation is described in the “Daidalos language” (DaidaL), which is especially developed for this purpose. The preparation time is greatly reduced by providing language constructs for the creation of

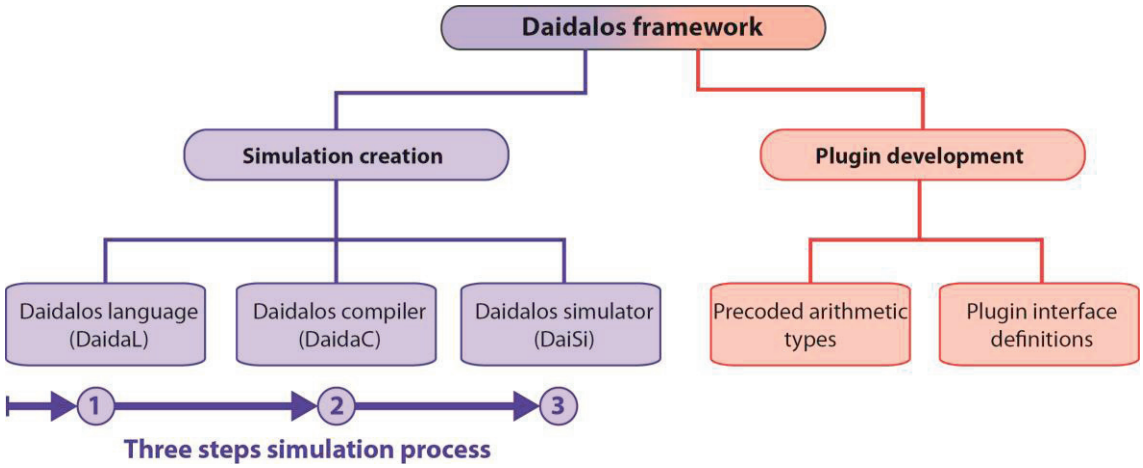

Fig. 2. A schematic overview of the structure of the DAIDALOS ray tracing framework. The framework provides support for the simulation design process (blue), by providing a three step process. On the other hand, plugin development (red) is supported by, amongst others, pre-coded arithmetic types and plugin interface definition.

geometry by means of constructive solid geometry (CSG), and for plugin applications. (ii) Using the "Daidalos compiler" (DaidaC) the DaidaL script is converted into a package format, which contains all plugins required by the simulation and may be easily transferred between different computers. (iii) The created package is executed by the "Daidalos simulator" (DaiSi) which, at this moment, provides a console interface, enabling the execution at a local workstation as well as by a remote connection, e.g. secure shell (SSH).

2.2. Plugin development

There are several predefined plugin interfaces provided, from which a developer may choose the one most suitable for the desired plugin functionality. These include standard effects such as light sources, as well as more abstract ones such as face effect, volume effects or refraction calculators. For further simplification, the framework provides a set of pre-coded, tested objects which may be readily used by any developer. Amongst others, this includes arithmetic types, e.g. matrices, vectors and complex numbers. By relying on these already verified objects, an accelerated development process can be achieved.

3. LBIC Measurement of a test module

Fig. 3 shows a light-beam induced current (LBIC) color code map of part of a minimodule consisting of 3×3 cells. The scan was performed with the solar cell analysis system LOANA [10]. Only the cell in the center is contacted (the right cell on the image), meaning that the left neighbor cell on the image is not contacted. There is a considerable signal when the light impinges on the neighbor cell or in the gap between cells, showing that light may travel distances of centimeters in modules until it is absorbed. For example, only part of the light impinging on a front metal finger is reflected back to the sky; a considerable part of light is reflected at an angle larger than about 45° from the normal, so it undergoes total internal reflection at the glass/air interface of the module and impinges on the cell or the gap region

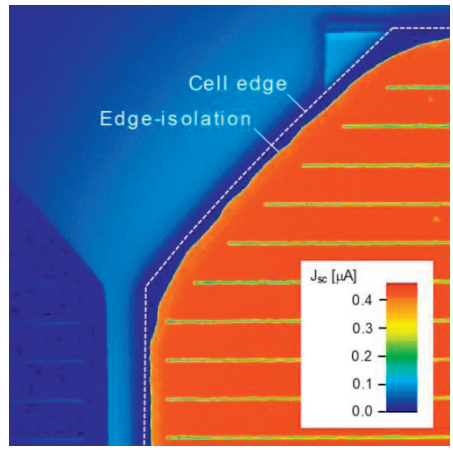

Fig. 3. Light-beam induced current (LBIC) scan, measured with the LOANA system [10], of a part of a module where the right cell is contacted to monitor *J*sc, and the left cell is not contacted. Note that the LBIC signal drops near the cell edge due to edge-isolation, causing a low collection efficiency of photo-generated carriers within the Si solar cell.

again. This implies that the optical losses are considerably smaller than the metal coverage [11-12], by a factor called the shading factor, which is 41.9% for screen-printed metal fingers in a module [12]. In Fig. 3, the metal fingers of the non-contacted cell are well visible because part of the reflected light finally enters the contacted cell. Similar arguments hold in the gap: if light impinges in the gap region close to a cell, a single internal reflectance at the glass/air interface is sufficient to deflect the light onto the cell; in gap regions further away than about double the glass thickness, more than one internal reflectance is necessary, making far gap regions appear darker in Fig. 3. Note that the signal is larger when light impinges on the cell interconnect ribbon. The higher reflectivity of the metal, compared to the backsheet, outweighs the smaller degree of scattering on metal surfaces

4. Ray tracing of PV modules

The described experiment indicates the demands on a ray tracer. Light may travel many centimeters while the cells are covered with pyramids in the micrometer range. The gap between the cells usually is 2 – 4 mm wide and contains cell interconnect ribbons, while the top and bottom edge of the module is 2 cm and 3.5 cm wide, respectively, containing the string interconnects. Such extended geometries would be very difficult to handle in a ray tracer even with today's computer capacities and speed. Therefore, we introduce a multi-domain approach as follows.

If we start a ray from top of a cell, the ray is traced as usual within the well-known domain shown in Fig. 4(a), where it may bounce between the symmetry-sidewalls back and forth many times. However, while doing so, a plug-in calculates the ray's *global* position r_g, and the plug-in tests whether the ray stays – from a global view point – within the cell. If r_g reaches the outermost pyramid at the cell's edge, the tracing of the ray is continued automatically in a second simulation domain shown in Fig. 4(b) and, hence, the ray may enter the gap region. If r_g of the ray enters the cell region again after a few bounces in the gap region, the tracing may be continued again in the domain of Fig. 4(a), and so forth. The simulation of a complete module requires a few gap domains shown in Fig. 4(b): a 2 mm wide gap between neighboring cells, a 1 cm wide gap at the side edges of the modules, some containing Sn60Pb40

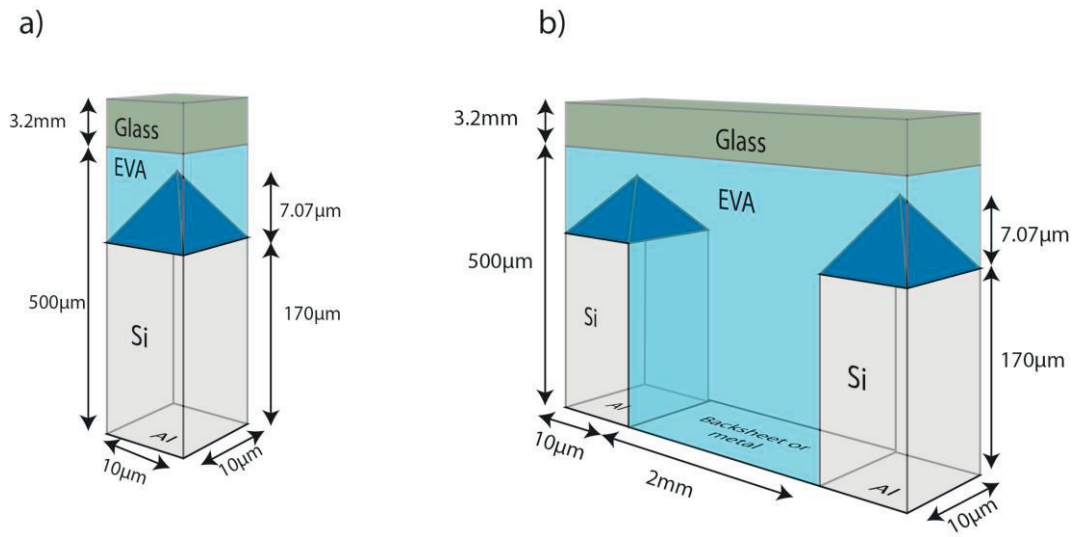

Fig. 4. (a) The simulation domain used for the solar cell; (b) the "gap domain", containing the inter-cell gap as well as the adjacent unit-domains of the cells. During a simulation of a solar cell module, the ray automatically switches between the domains when the ray's global coordinate reaches the outermost pyramids at a cell's edge.

ribbons, etc. With this approach, we are able to simulate complete modules by including only a few different simulation domains, keeping the computing requirements to a manageable size.

4.1. Optical and geometrical data

In the solar cells, we choose the wavelength-dependent refractive index n and extinction coefficient k for crystalline silicon from Ref. [13]. We use our own measurements for the 76 nm thick SiN_x antireflection coating, which has $n = 2.05$ at the wavelength of 633 nm. The full-area rear metal contact is an aluminiumsilicide (AlSi) eutectic [14]. As we have not found precise n and k data for AlSi in the literature, we resort to the effective medium theory by interpolating between 13.6 volume % of Si [13] and Al [15]. The optical data for ethylene vinyl acetate (EVA) are taken from Ref. [13]. The reflectivity of the backsheet materials were measured in-house as shown in Fig. 5. In the ray tracer, we assume Lambertian reflection at the backsheet. The data for the ribbons, covered with an Sn60Pb40 alloy, are taken from Ref. [17] and we assume in the ray tracer that a fraction of 0.2 reflects in a Lambertian manner. There is an antireflection coating on top of the front glass, which has $k = 0$ and n equal to 0.9 of the n of glass. These fictive n values come close to the values we measured in-house from commercial manufacturers.

4.2. Ray tracing of LBIC measurement

As a first simulation example, let us follow the light-source of the LBIC set-up as it moves from the cell toward the gap in Fig. 6. If the light-source is positioned on top of the cell, the generation current-density J_{gen} is almost unaffected by the gap's existence, as shown at negative space coordinates. Only if the light-source comes very close to the cell's edge, part of the incoming photons is reflected into the gap region, leading to a moderate reduction in J_{gen}. As soon as the light-source reaches the gap, J_{gen} drops by a

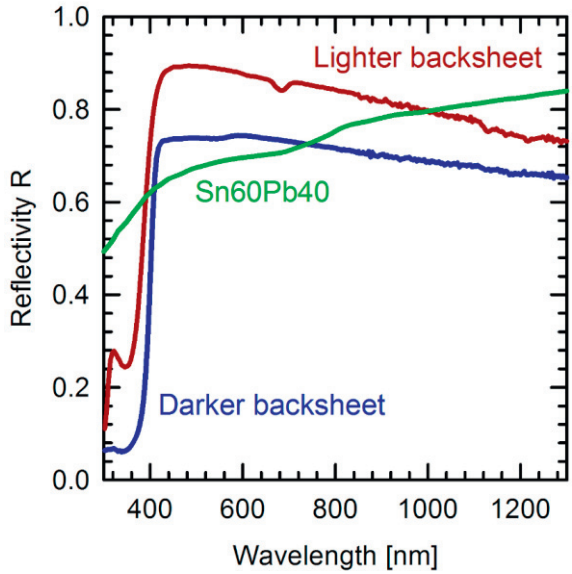

Fig. 5. The diffuse reflectivity of two different commercially available backsheets and of a cell interconnection ribbon covered with a tin and lead alloy.

factor of approximately two. As long as the light source is still very close to the cell, part of the rays is directly reflected onto the cell edge (the rays labeled 1) and causes the decrease in J_{gen} shown in Fig. 6(a). When the light-source moves further away from the cell's edge, J_{gen} stays rather constant. This plateau exists because rays can reach the cell by a single internal reflection at the front glass/air interface. With increasing distance from the cell's edge, J_{gen} keeps dropping further, as shown in Fig. 6(b). This is so because the rays are reflected upwards from the backsheet in fully randomized directions. The angle of total reflection at the glass/air interface is 45°, so about two thirds of the reflected rays stay in the module and possibly hit the cell (the rays labeled 2 in the drawing of Fig. 6(b)). If the light-source moves further away from the cell edge than double of the thickness of the front module glass, a growing part of rays needs to be reflected twice at the glass/air interface to reach the cell and to contribute to J_{gen}. Each time the rays are reflected again at the backsheet, about one third escapes into the sky. Therefore, J_{gen} decreases even further.

In order to directly compare the LBIC measurements and ray tracing, we need to be aware that LBIC monitors the short-circuit density J_{sc}, which is J_{gen} times the cell's carrier collection efficiency η_c. To compare the ray traced J_{gen} with the measured J_{sc}, we need to scale J_{sc} by η_c. We obtain η_c from numerical device simulations. The results are shown in Fig. 7 as red symbols. The agreement between ray tracing and LBIC is good far away from the cell. Close to the cell, the LBIC signal drops because there is an unusually large cavity between backsheet and cell due to the rear metal contacts, so part of the rays is reflected from the backsheet to the back of the cell. From the comparison between ray tracing and LBIC, it is apparent that this cavity causes optical losses just where the rays could reach the cell's front surface with one single reflection at the glass/air interface. In the ray trace simulation the back sheet is assumed to be directly behind the solar cell. So this effect cannot be seen in the simulation. Therefore the generation current of the simulation is higher than in the measurement close to the cell. This implies that the cavity needs to be minimized.

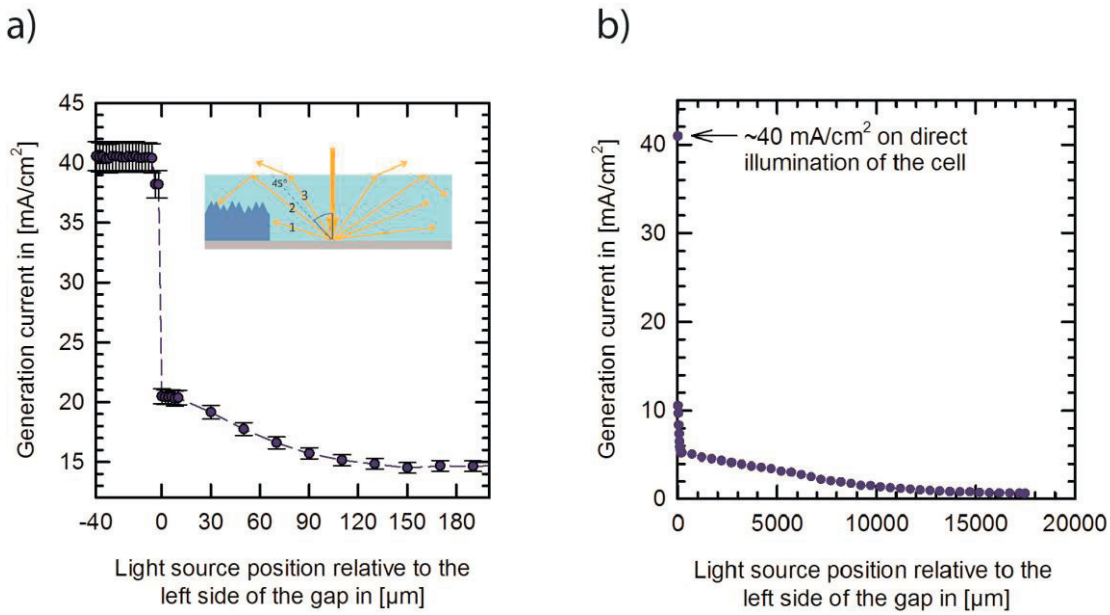

Fig. 6. Ray traced generation current density Jgen in dependence of the position of the light-source within the gap between two neighboring cells. The position 0 µm marks the edge of the solar cell. In (a), Jgen drops with distance to the cell edge because a smaller fraction of rays (labeled 1 in the drawing) directly hits the cell. Further away from the cell's edge, in (b), Jgen keeps dropping further because the number of rays labeled 2 decrease with increasing distance from the cell's edge.

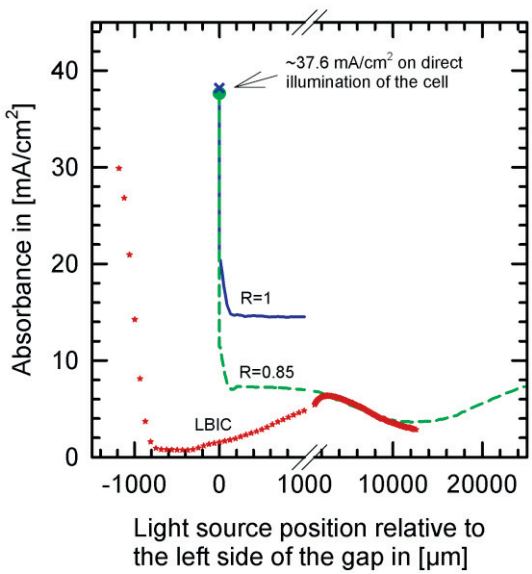

Fig. 7. Comparison of the LBIC experiment of Fig. 3 with ray tracing, using a perfectly reflective and a commercially available backsheet, respectively. The LBIC signal is converted to absorbed photon flux with a simulated carrier collection efficiency within the solar cell.

References

[1] T. Uematsu, M. Ida, K. Hane, Y. Hayashi and T. Saitoh. A new light-trapping structure for very thin, high-efficieny silicon solar cells. In *Proc. 20th IEEE PV Specialists Conference*; 1988, Las Vegas, NV, p. 792

[2] A.W. Smith, A. Rohatgi, S. C. Neel. Texture: a ray tracing program for the photovoltaic community. In *Proc. 21st IEEE PV Specialists Conference;* 1990, Kissimmee, FL, p. 426.

[3] R. Brendel. Simple prism pyramids: a new light trapping texture for silicon solar cells. In *Proc. 23rd IEEE PV Specialists Conference;* 1993, Louisville, KY, p. 252.

[4] J. Schumacher, S. Sterk, B. Wagner, W. Warta. Quantum efficiency analysis of high efficiency solar cells with textured surfaces. In *Proc. 13th EPSEC*; 1995, Nice, France, p. 96.

[5] C. Zechner, P. Fath, G. Willeke, E. Bucher. Numerical simulation studies of mechanically textured high efficiency silicon solar cells. In *Proc. 14th EPSEC*, 1997, Barcelona, Spain, p. 69.

[6] J. E. Cotter. Raysim 6.0 – a free geometrical ray tracing program for silicon solar cells. In: *31st IEEE PV Specialists Conference*, 2005, Lake Buena Vista, FL, p. 1165.

[7] K.R. McIntosh, R.M. Swanson and J.E. Cotter. A simple ray tracer to compute the optical concentration of photovoltaic modules. *Progress in Photovoltaics* 2006;**14**,167.

[8] K.R. McIntosh, OPAL and TRACEY, available at www.pvlighthouse.com.au.

[9] P. Grunow, and S. Krauter. Modeling of the encapsulation factors for photovoltaic modules. In *Proc. 4th World Conference on Photovoltaic Energy Conversion*, 2006,Waikoloa, Hawaii, p. 2152.

[10] Solar cell analysis system LOANA from PVtools GmbH, Hameln, Germany.

[11] M.F. Stuckings and A.W. Blakers. A study of shading and resistive loss from the fingers of encapsulated solar cells". *Solar Energy Materials and Solar Cells* 1999;**59**, 233.

[12] R. Woehl, M. Hörteis, S. W. Glunz. Determination of the effective optical width of screen-printed and aerosol-printed and plated fingers. In *Proc. 23rd EPSEC*, 2008, Valencia, Spain, p. 1377.

[13] M. A. Green. Self-consistent optical parameters of intrinsic silicon at 300K including temperature coefficients. *Solar Energy Materials and Solar Cells* 2008; **92**, 1305.

[14] A. Ingenito, O. Isabella, M. Zeman. Accurate opto-electrical modeling of multi-crystalline silicon wafer-based solar cells. In *Proc. 27th EPSEC*, 2012, Frankfurt, Germany, p. 1208.

[15] E. Shiles, T. Sasaki, M. Inokuti, and D. Smith. Self-consistency and sum-rule tests in the Kramers-Kronig analysis of optical data: Applications to aluminum. *Physical Review B*, 1980; **22**, 1612.

[16] K. R. Mcintosh, N. E. Powell, A. W. Norris, J. N. Cotsell, and B. M. Ketola. The effect of damp-heat and UV aging tests on the optical properties of silicone and EVA encapsulants. *Progress in Photovoltaics*, 2010; **19**, 294.

[17] M. Gast, M. Köntges, R. Brendel. In-laminate laser soldering – A gentle method to assemble and interconnect silicon solar cells to modules. In *Proc. 21st EPSEC*, 2006, Dresden, Germany, p. 2133.